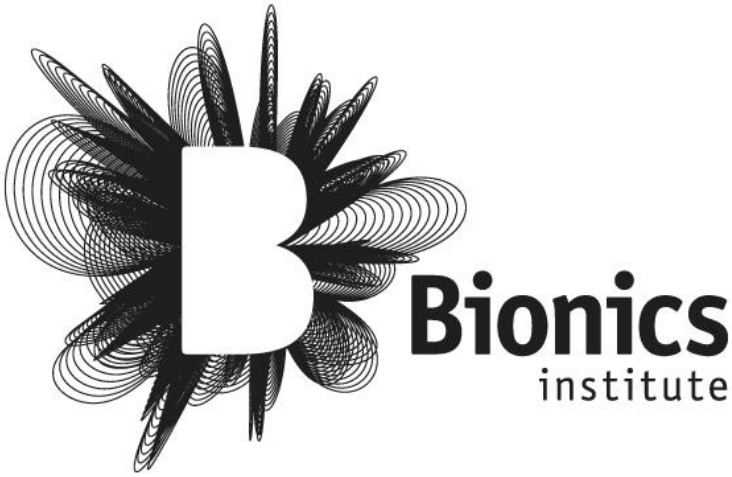

Inferior Colliculus Responses to Dual-site Intra-Lamina Stimulation in the Ventral Cochlear Nucleus

Mohit N. Shivdasani[1,2,3], Stefan J. Mauger[1,2,3], Rebecca E. Argent[2], Graeme D. Rathbone[2,3] & Antonio G. Paolini[1,2]

[1]School of Psychological Science, La Trobe University, VIC – 3086, AUSTRALIA

[2]The Bionic Ear Institute, East Melbourne, VIC – 3002, AUSTRALIA

[3]Department of Electronic Engineering, La Trobe University, VIC – 3086, AUSTRALIA

Running Head: Dual Stimulation in the Ventral Cochlear Nucleus

Supporting Grants: Garnett Passe & Rodney Williams Memorial Foundation: Project Grants 2005, 2007

Keywords: Auditory Brainstem Implant, Neural Prostheses, Electrical Stimulation, Auditory Brainstem, Auditory Midbrain

Corresponding Author:

A/Prof. Antonio Paolini
Graeme Clark Centre for Bionic Ear and Neurosensory Research
School of Psychological Science
La Trobe University
Bundoora
Victoria – 3086
AUSTRALIA
Tel: +61-3-94792947
Fax: +61-3-94791956

Abstract

A major limitation of the present auditory brainstem implant (ABI) is its inability to access the tonotopic organization of the ventral cochlear nucleus (VCN). A previous study by our group indicated that stimulation of single sites within a given VCN frequency region did not always elicit frequency-specific responses within the central nucleus of the inferior colliculus (CIC) and, in some cases, did not elicit a response at all. In this study, we hypothesized that sequential stimulation (with a short inter-pulse delay of 320 μs) of two VCN sites in similar frequency regions would enhance responsiveness in CIC neurons. Multiunit neural recordings in response to pure tones were obtained at 58 VCN and 164 CIC sites in anesthetized rats. Of the 58 VCN sites, 39 pairs of sites with similar characteristic frequencies were chosen for electrical stimulation. Each member of a VCN pair was electrically stimulated individually, followed by sequential stimulation of the pair, while recording CIC responses. On average, CIC sites were found to respond to dual-site VCN stimulation with significantly lower thresholds, wider dynamic ranges, a greater extent of activation with increasing current levels, and a higher degree of frequency specificity compared to single-site stimulation. While these effects were positive for the most part, in some cases dual-site stimulation resulted in increased CIC thresholds and decreased dynamic ranges, extent of activation, and frequency specificity. The results suggest that multi-site stimulation within VCN isofrequency laminae using penetrating electrodes could significantly improve ABI stimulation strategies and implant performance.

Introduction

The auditory brainstem implant (ABI) is used to restore hearing in patients who are unable to benefit from a cochlear implant (CI). Presently, this is achieved through surface stimulation of the ventral cochlear nucleus (VCN) in the auditory brainstem (Colletti et al., 2004a; Colletti et al., 2004b; Colletti et al., 2005; Colletti et al., 2004c; Colletti and Shannon, 2005; Jackson et al., 2002; Kuchta, 2007; Otto et al., 2002; Otto et al., 1998; Schwartz et al., 2008). This surface ABI has had limited clinical success, a result attributable, in part, to its inability to access the tonotopic organization of the VCN, which is thought to be a crucial element for speech perception (Kuchta et al., 2004; Schwartz et al., 2008). It has been proposed that penetrating electrodes may be able to stimulate localized regions of the VCN and thus provide better access to its tonotopic organization (McCreery et al., 2007; McCreery, 2008; McCreery et al., 1998).

Several electrophysiological studies in animals have demonstrated that stimulation via penetrating electrodes in the VCN can produce activation in higher order auditory brain centers with low thresholds, wide dynamic ranges and a high degree of frequency specificity. (El-Kashlan, 1999; El-Kashlan et al., 1991; Liu et al., 1997; Liu et al., 1998; McCreery et al., 2007; McCreery et al., 1998; Niparko et al., 1989a; Niparko et al., 1989b; Shivdasani et al., 2008; Takahashi et al., 2005). Recent reports from the first ten human patients who received a penetrating auditory brainstem implant (PABI) have indicated that auditory perception thresholds were significantly lower than those obtained with the surface array, and that the penetrating arrays were better able to access the tonotopic organization of the VCN (McCreery, 2008; Otto et al., 2008). However, simply incorporating penetrating electrodes in addition to surface electrodes in a single array design, as in the case of the PABI, was not sufficient to guarantee

favorable results. The patients fitted with the PABI did not perform better as a group on speech recognition tasks than patients implanted only with a surface array (McCreery, 2008; Otto et al., 2008). It is likely that conventional CI-based stimulation strategies used in both the ABI and PABI may have significantly contributed to the limited clinical performance observed, indicating a significant need to develop novel stimulation strategies.

Our recent animal experiments have demonstrated the complexity involved in stimulating the VCN with a PABI. We showed that placement of the PABI array was a critical factor in producing frequency-specific activation of the central nucleus of the inferior colliculus (CIC) and that stimulation of single VCN sites did not always elicit a response in the CIC within safe charge-density limits (Shivdasani et al., 2008). In another study, we found that VCN neurons within similar frequency regions exhibited strong synchronization characteristics in response to an acoustic stimulus (Shivdasani et al., 2009). Based on these results, we propose that stimulation of single VCN sites, as employed in current ABIs, may not be sufficient to achieve the optimum frequency specificity necessary for understanding speech. Simultaneous stimulation of multiple sites within VCN isofrequency laminae may be required to improve speech perception with an ABI. In this investigation, we undertook the first step towards understanding how to implement multi-site stimulation. We examined whether dual-site stimulation within a VCN isofrequency lamina would result in lower thresholds, wider dynamic ranges, an increased extent of activation, and a higher degree of frequency specificity in the CIC, compared to single-site stimulation. Lower thresholds of activation would result in safer stimulus levels for patients. Higher dynamic ranges (Loizou et al., 2000;

Zeng and Galvin, 1999) and higher frequency specificity (Friesen et al., 2001; Shannon et al., 2004) could together contribute to better speech perception.

Materials and Methods

Surgery and Electrode Insertion

Male Hooded Wistar rats (n = 7, Flinders University, Adelaide, SA, Australia) weighing 350-450 gm were anesthetized with Urethane/dH_20 (20% w/v, Sigma Aldrich, NSW, Australia). The animals were placed in a stereotaxic frame (David Kopf Instruments, Tujunga, CA) fitted with hollow ear bars. Animal temperature was monitored continuously and maintained at 37^oC using a DC temperature controller (Model ATC1000, World Precision Instruments, Inc., Sarasota, FL). Craniotomies were performed to expose the left VCN and the contralateral inferior colliculus (IC). The cerebellum was partially aspirated to expose the VCN. Under visual control, 32-channel electrodes (Neuronexus Technologies, Ann Arbor, MI) were inserted into the VCN and the contralateral CIC along their respective tonotopic axes. Each electrode consisted of four silicon substrate shanks (200 μm apart), with eight iridium electrode sites (413 μm^2 surface area, 200 μm apart) on each shank. All experimental procedures were approved by the St. Vincent's Hospital Animal Ethics Committee (Protocol 35/06).

To increase their charge storage capacity for electrical stimulation, VCN electrode sites were electrochemically activated by cyclic voltammetry using a standard three-electrode potentiostat (660B Potentiostat and CHI200 Picoamp Booster, CH Instruments, Inc., Austin, TX) prior to each experiment. The activation procedure, involving conversion of iridium to iridium oxide (Anderson et al., 1989), reduced the impedance of each VCN site from approximately 1 MΩ to less than 100 kΩ measured at 1 kHz. Each CIC electrode site (not activated) had an impedance of 1-3 MΩ measured at 1 kHz.

In all animals, the VCN electrodes were inserted at a 30 degree caudo-rostral angle in order to access the central parts of the posteroventral cochlear nucleus (PVCN),

electrical stimulation in which is known to elicit highly frequency-specific responses in the CIC. (Shivdasani et al. 2008). The CIC electrodes for all experiments were inserted at a 10 degree rostro-caudal angle. A low impedance silver reference electrode placed under the skin served as a reference for action potential recording.

Immediately prior to electrode insertion, both the VCN and CIC electrodes were coated with fluorescent stain (DiI; 1, 1-dioctadecyl-3,3,3′,3′-tetramethyindocarbocyanine perchlorate; CAT D3911; Molecular Probes, Eugene, OR; 2.5 mg/ml in absolute ethanol) to allow histological confirmation of electrode placement. Similar protocols have been previously described by DiCarlo et al. (1996), Lim and Anderson (2007) and Mauger et al. (2010).

Acoustic Protocols

Stimulus generation and data acquisition were performed using Tucker Davis Technologies System III hardware (TDT, Alachua, FL) with a custom-designed software package. The electrodes were advanced using a motorized micro-drive (Sutter Instruments, Novato, CA) and acoustically evoked multiunit activity within the VCN and CIC was detected by presenting 50-ms white noise bursts (rise-fall time 5 ms; 500-ms inter-stimulus interval; Gaussian distributed noise, 1 – 44 kHz). Once the electrodes were in position, neural responses to 50-ms pure tone bursts (rise-fall time 5 ms; 300-ms inter-stimulus interval) of varying frequency (1 – 44 kHz in 1 kHz steps) and amplitude (10 – 70 dB sound pressure level (SPL) in 10 dB steps) were recorded. Each frequency-SPL combination was presented 10 times. These data were used to determine an acoustic response area (RA) and characteristic frequency (CF; frequency at which threshold was lowest) for each VCN and CIC recording site.

All auditory stimuli were calibrated prior to each experiment using a 1/8-inch Brüel & Kjær microphone and measuring amplifier unit (Nærum, Denmark). Calibration was performed with a speaker attached to one end of the ear bar with the microphone and amplifier unit coupled to the other end using a 3 mm long rigid plastic tube to mimic the rat's ear canal.

Electrical Protocols

Pairs of VCN sites with similar CFs were chosen for electrical stimulation. During electrical stimulation (single and dual), the site on the electrode shank directly above a given stimulating site was used as the return. Each member of a VCN pair was stimulated separately with cathodic-leading, charge-balanced, biphasic current pulses (120 μs per phase, 80-μs interphase gap, bipolar configuration) at a rate of one pulse every 500 ms (2 Hz). Current levels were increased from 1 to 54 μA (1 to 15 μA in 1 μA steps; 18 to 54 μA in 3 μA steps) with 20 repetitions at each current amplitude. Following single site stimulation, the two VCN sites were stimulated sequentially in an interleaved fashion (320 μs between onsets of pulses). The current levels at both sites were increased simultaneously, using the same current steps as for single-site stimulation. This technique of interleaved stimulation rather than simultaneous stimulation was used to avoid complex effects of channel interaction (Bierer and Middlebrooks, 2004; Loizuo, 1998; Nobbe et al., 2007; Stickney et al., 2006). Using a low pulse rate and a low maximum current level ensured that we did not damage the electrode sites (Beebe and Rose, 1988) or neural tissue (McCreery et al., 1990). At the end of the stimulation paradigm, the acoustic RA protocols were repeated to ensure that

VCN neurons were still functional and showed similar tuning properties to those observed before electrical stimulation.

Data Acquisition

Neural data were acquired at a sampling rate of 24.4 kHz using an online threshold-based spike discriminator. The incoming signal on each channel was monitored in a two-second window to estimate the spontaneous baseline level of activity. If the signal crossed the baseline activity by more than 4.2 standard deviations, a spike detector was triggered and the next 31 samples (total duration 1.2 ms) of the signal waveform were recorded (bandpass filtered from 300 - 5000 Hz). This 1.2-ms sample will be termed a spike snippet. A timestamp value that indicated the time of the largest positive or negative peak of the action potential was also recorded. After recording a spike snippet, the spike detector could be triggered again.

Data Analysis

To provide a more accurate estimate of spike occurrence, system-acquired spike snippets were processed offline in Matlab (The Mathworks, Inc., Natick, MA). Multiple action potentials were extracted from each system-acquired spike snippet using a re-thresholding procedure (see Shivdasani et al. 2008, 2009). Spike sorting of multiunit activity into single units was not performed.

Spike rate was calculated (using a time window of 0 – 50 ms from stimulus onset) for each tonal frequency-SPL combination presented, and plotted as a function of frequency and SPL to generate an acoustic RA for each recording site in the two structures (examples shown in Fig. 2 and Fig. 3). Acoustic RAs were constructed using three-

dimensional, color-filled contour plots (Sigmaplot 8.0, Systat Software, Inc., San Jose, CA). The colors of the acoustic RAs were smoothed using standard linear interpolation (Sigmaplot 8.0, Systat Software, Inc., San Jose, CA). Acoustic threshold was determined as the lowest SPL at which spike rate during the stimulus window (0 – 50 ms) was at least twice that in a post-stimulus time window (50 – 100 ms), and CF was defined as the frequency at which threshold was lowest

The spike rate for CIC responses to electrical stimulation was calculated using a window of 2 – 35 ms after stimulus onset, to ensure that the stimulus artifact recorded in the CIC was excluded. Electrical rate-level functions were generated for each CIC site in response to single and dual-site VCN stimulation by plotting spike rate as a function of current amplitude. The rate-level functions were used to estimate thresholds and saturation points with a resolution of 0.5 μA by using a well established method in auditory system research (Koppl and Yates, 1999; Nizami, 2002; Sachs and Abbas, 1974; Sachs et al., 1989; Shivdasani et al., 2008; Yates et al., 2000; Yates et al., 1990). Specifically, a least-squares regression method was used to fit a sigmoid to the electrical rate-level functions. Endpoints of the dynamic range were determined by calculating the current levels required to produce firing rates 10% above threshold and 10% below saturation (Nizami, 2002; Yates et al., 2000). The threshold and saturation estimates obtained using these methods were strongly correlated with the values obtained by visual inspection of the electrical peri-stimulus time histograms. Both antidromic and orthodromic spikes were included in our analyses. We have previously shown that antidromic spikes have negligible effects on spike threshold and saturation point calculations (Shivdasani et al. 2008).

Histology

At the conclusion of each experiment, the animal was deeply anesthetized and perfused transcardially with 4% paraformaldehyde (PFA, Electron Microscopy Sciences, Hatfield, PA) in 0.1 M phosphate buffered saline (PBS, pH 7.4). Brains were stored in 0.4% PFA/PBS then transferred to a cryo-protectant solution of 30% sucrose/PBS prior to sectioning. Full brain serial sections (60 μm thickness) were cut in the coronal plane using a cryostat (Leica CM 1850, Leica Microsystems, Wetzlar, Germany). Sections were collected on super-frost slides and stained with NeuroTrace Fluorescent Nissl stain: 500/525 (CAT N21480; Molecular Probes, Eugene, OR). Positions of the electrodes within the VCN (marked by the DiI stain) were confirmed and photographed using fluorescent microscopy (Nikon Eclipse 90i Microscope & Nikon DS-SMC digital camera, Nikon Corporation Instruments Company, Kanagawa, Japan). Photomicrographs were compiled from separate red and green channel images and modified to increase contrast in the green channel only, using Adobe Photoshop CS (v8.0, San Jose, CA). We were able to determine the VCN probe placement for each experiment (Fig. 1) by comparing histological images with a rat brain atlas (Paxinos and Watson, 2007).

Results

Histological Analysis

Schematic diagrams of VCN electrode placements were constructed from histological sections and showed the location of individual electrode shanks and sites in both the horizontal (Fig. 1A) and parasagittal planes (Fig.1B-H, left panels). Tonotopic maps were constructed and confirmed the high-to-low frequency gradient of CFs along the dorso-ventral axis of the VCN (Fig. 1B-H, right panels). Histological analysis confirmed that the majority of electrode shanks entered the PVCN (Fig. 1A). Although the central regions of the PVCN were targeted, in two experiments a number of electrode sites were located in the dorsal CN (DCN) or close to the DCN-VCN border (see Fig. 1D and H). These sites were not used for electrical stimulation. Histology was also performed on the IC (not shown) to confirm the location of electrodes. In all cases, electrode shanks were located in the central nucleus; a standard stereotaxic atlas of the rat brain was used as a reference (Paxinos and Watson, 2007).

Classification of VCN and CIC Sites

A total of 58 VCN sites from a total of 224 possible sites (7 animals, 32 sites per animal) were used for single-site stimulation The remaining 166 VCN sites were not used for electrical stimulation because they did not show any multiunit activity in response to acoustic stimulation (open circles in tonotopic maps, Fig. 1B-H), were located outside the VCN, or could not be paired with a similar CF site for dual-site stimulation. A total of 164 of 224 CIC sites showed multiunit activity in response to

acoustic stimulation, and their responses to VCN electrical stimulation were used for data analyses.

The first step was to determine the frequency specificity of the activity elicited in the CIC by stimulation of each of the 58 VCN sites chosen for single-site stimulation. To do this, the CIC sites that responded with the lowest thresholds to stimulation of each VCN site were identified, and the CFs of those CIC sites were then used as the basis for determining the frequency specificity of that VCN site. If all the lowest-threshold CIC sites had CFs that were within 1/8 of an octave of the CF of the stimulated VCN site (and/or the CF of its corresponding return), that VCN site was classified as "frequency-specific" (FS) and the CIC sites were classified as "CF-aligned". Thirty seven of the 58 VCN sites fulfilled this criterion and were classified as FS. The remaining VCN sites were classified as non-frequency-specific (NFS; n = 21). As bipolar stimulation was employed in this study, it was possible for the leading cathodic phase of each current pulse to stimulate neurons close to a given VCN site, while the reversal, anodic phase could stimulate neurons close to the return. Hence, assessment of the CFs of the lowest threshold CIC sites in relation to the CFs of both the stimulated VCN site and its return (located directly above) was essential.

A total of 39 pairs of VCN sites with similar CFs (maximum difference of 2 kHz) were chosen for dual-site stimulation (a single VCN site could be used in more than one pair). These VCN pairs were classified as FS-FS pairs (n = 16; both VCN sites were FS with single-site stimulation), FS-NFS pairs (n = 15; one of the VCN sites was FS, the other NFS with single-site stimulation) or NFS-NFS pairs (n = 8; both VCN sites were NFS with single-site stimulation). As for single-site stimulation, a given VCN pair was deemed to be frequency-specific only if all the lowest threshold CIC sites activated by

stimulation of that VCN pair were CF-aligned to that VCN pair (and/or their respective returns).

In a given experiment, it was possible for a CIC site to respond to stimulation of more than one VCN pair. Therefore, each CIC site's response to single- and dual-site stimulation of a given VCN pair was classified as a CIC response set. Since there were multiple possible combinations of responding CIC sites and stimulated VCN sites and pairs, a total of 885 CIC response sets were analyzed and classified into five groups as outlined in Table 1. As the focus of this study was to analyze and compare CIC responses to single- and dual-site VCN stimulation, only Group 1 CIC response sets were used for further analyses. Group 1 response sets (n = 606, 68.5%) comprised CIC sites that responded to stimulation of the two individual VCN sites comprising a pair and also responded to dual-site stimulation of the pair, at any current level below the maximum level used (54 μA). These CIC response sets were further classified into CF-aligned and CF-unaligned response sets (n = 312 and n = 294, respectively). The former consisted of sets in which the CIC sites had CFs that differed by less than 1/8 of an octave from the CFs of the stimulated VCN sites (and/or their respective returns), while the latter consisted of sets in which the VCN and CIC CFs differed by more than 1/8 of an octave.

Multi-peaked Tuning in the CIC

Previous recordings in the CIC of the rat (Hernandez et al., 2005) and mouse (Portfors and Felix, 2005) have shown that in addition to neurons that exhibit typical "V-shaped" acoustic RAs, a significant proportion of CIC neurons exhibit a variety of other "non V-

shaped" RAs. We classified the RAs at CIC sites (n = 164) into three groups, as illustrated in Fig. 2: those that were V-shaped and had a single peak (CF) (48.2%, n = 79; Fig. 2A), those that were multi-peaked with one peak at CF and a second peak with a higher threshold at another frequency (31.7%, n = 52; Fig. 2B), and those that had a complex RA (20.1%, n = 33; Fig. 2C). In order to classify multi-peaked RAs accurately, and to distinguish them from single peaked RAs, we used criteria similar to those described by Hernandez et al. (2005) and Sutter and Schreiner (1991). Specifically, the acoustic thresholds of the two peaks forming the multi-peaked RA had to differ by 40 dB SPL or less, and the frequency separation between the peaks had to be maintained at a level that was at least 10 dB SPL above minimum acoustic threshold.

Multi-peaked CIC RAs were found to influence the identification of VCN sites as either FS or NFS. Twelve of 52 (23.1%) CIC sites with multi-peaked RAs were found to respond with lowest threshold to VCN stimulation when the frequency of the *non*-CF peak was within 1/8 of an octave of the CF of the stimulated VCN site or pair (and/or their corresponding returns). According to our definition of frequency specificity, the VCN sites in these cases would normally be classified as NFS. However, we classified the VCN sites that showed this behavior as FS. CIC sites with complex RAs did not respond with lowest threshold to stimulation of any of the VCN sites/pairs and these sites did not influence the identification of VCN sites as either FS or NFS.

Effects of Single- versus Dual- Site VCN Stimulation on CIC Responses

Thresholds, Saturation Points and Dynamic Ranges

Figure 3 (A-C) shows the acoustic RAs at two VCN sites and at a CF-aligned CIC site for a representative response set. Figure 3D shows the effect of dual-site stimulation on CIC threshold compared to single-site stimulation of the two VCN sites. As illustrated by this example, the CIC site responded to single-site stimulation of the individual VCN sites with different thresholds, and to dual-site stimulation with an overall lower threshold.

Figure 4 shows the mean thresholds, saturation points and dynamic ranges of CF-aligned and CF-unaligned CIC sites in response to single- and dual-site stimulation for all VCN pairs and each of the pair types (FS-FS, FS-NFS and NFS-NFS). A three-factorial (2 x 2 x 3) repeated-measures analysis of variance (ANOVA, computed using an alpha of 0.05; Hinkle et al., 1998) was performed for each response measure (threshold, saturation point and dynamic range), with stimulation type (single or dual) and CF-alignment status (aligned or unaligned) as within-subject factors, and pairing type for dual-site stimulation (FS-FS, FS-NFS or NFS-NFS) as a between-subjects factor.

In the analysis of the threshold data, a significant reduction in mean threshold was found for dual-site compared to single-site VCN stimulation for both CF-aligned and CF-unaligned CIC sites, regardless of the type of pairing (Fig. 4A-D) ($F(1,263) = 66.823$, $p < 0.0001$, ($\eta_p^2 = 0.203$)). There was a significant interaction effect between CF-alignment status and stimulation type ($F(1,263) = 9.776$, $p < 0.005$, ($\eta_p^2 = 0.036$)). A post-hoc simple effects analysis of this interaction revealed that CF-aligned thresholds

were significantly lower than CF-unaligned thresholds for dual-site stimulation but not for single-site stimulation. A significant interaction was also observed between CF-alignment status and the type of pairing ($F(2,263) = 9.069$, $p < 0.0001$, ($\eta_p^2 = 0.065$)). A post-hoc simple effects analysis showed that CF-aligned thresholds for stimulation of the FS-FS pairs differed significantly from those of the FS-NFS and the NFS-NFS pairs ($p < 0.05$). No significant interaction effect was observed between stimulation type and pairing type, and the three-way interaction was also non-significant.

Saturation points (Fig. 4E-H) of both CF-aligned and -unaligned CIC sites were significantly lower with dual-site stimulation than with single-site stimulation for all types of VCN pairs ($F(1,263) = 11.701$, $p = 0.001$, ($\eta_p^2 = 0.043$)). Saturation points of CF-aligned CIC sites were significantly lower than those of unaligned CIC sites for single- and dual-site stimulation ($F(1,263) = 7.405$, $p < 0.01$, ($\eta_p^2 = 0.027$)). A significant interaction was found between CF-alignment status and pair type ($F(2,263) = 14.889$, $p < 0.0001$, ($\eta_p^2 = 0.102$)). A post-hoc simple effects analysis showed that CF-unaligned saturation points for stimulation of the FS-FS pairs differed significantly from those of the FS-NFS pairs ($p < 0.05$). Interaction effects between CF alignment status and stimulation type for saturation points, and the three-way interaction, were found to be non-significant.

In contrast to threshold and saturation point, mean dynamic range (calculated in dB) was found to increase significantly with dual-site stimulation compared to single-site stimulation (Fig. 4I-L) ($F(1,263) = 62.919$, $p < 0.0001$ ($\eta_p^2 = 0.193$)). No interaction was found between pair type and stimulation type. A significant interaction was found between stimulation type and CF-alignment status ($F(1,263) = 4.55$, $p < 0.05$ ($\eta_p^2 = 0.017$)). A post-hoc simple effects analysis indicated that, for dual-site stimulation,

dynamic ranges of the CF-aligned and unaligned sites were not significantly different. The interaction between CF-alignment status and VCN pair type was significant ($F(2,263) = 4.769$, $p < 0.01$ ($\eta_p^2 = 0.035$)), and a post-hoc analysis showed that the dynamic ranges of CF-aligned sites were not significantly different from those of the unaligned sites for stimulation of the FS-NFS and NFS-NFS pairs. No significant interaction effect between stimulation type and VCN pair type was found, and the three-way interaction was also non-significant.

A more detailed analysis was performed to examine the variability observed in the thresholds and dynamic ranges of CIC neurons resulting from dual-site stimulation of the different VCN pair types. We analyzed the changes in CIC thresholds, saturation points and dynamic ranges associated with dual-site stimulation in relation to the physical separation between the two VCN sites forming each pair (Fig. 5). Dual-site stimulation resulted in decreased thresholds and wider dynamic ranges in the CIC for the majority of VCN pairs, but in some cases resulted in the opposite effect (negative values in Fig. 5). In cases where thresholds were found to increase with dual stimulation, they generally did so by less than or equal to 30%. Threshold reductions produced by dual-site stimulation were generally greater and extended up to 60% (Fig. 5D-F). Saturation points in both CF-aligned and -unaligned CIC sites were generally lower with dual-site stimulation (Fig. 5G-I), in some cases by up to 60% (Fig. 5J-L). Dynamic ranges generally increased by 1-8 dB with dual-site stimulation, but decreased by 1-5 dB in few cases (Fig. 5M-O). The benefits from dual-site stimulation, particularly the increased dynamic ranges, were more commonly observed in CF-aligned CIC sites than in unaligned sites.

It was important to rule out direct current summation effects as a factor in obtaining lower CIC thresholds and saturation points, and wider dynamic ranges, with dual-site stimulation, even though we used interleaved stimulation rather than simultaneous stimulation to avoid such summation effects. The physical separation between VCN stimulation sites for the FS-FS and the FS-NFS pairs did not appear to influence the improvement in threshold or dynamic range in CIC neurons (for either CF-aligned or unaligned sites). This was not the case for the NFS-NFS pairs (Fig. 5C, F, and O), in which there was a systematic decrease in the threshold improvement with increasing separation between the VCN stimulation sites (Fig. 5C and F). A similar trend was observed in the dynamic range data (Fig. 5O) although it was not as marked.

Rate-Level Functions

A variety of rate-level functions were recorded from CIC multiunit clusters in response to VCN stimulation. The shape of the rate-level function was used to classify multiunit cluster responses into four categories: monotonic (spike rate did not saturate within the range of stimulus levels presented), plateau (spike rate increased monotonically with increasing current levels and then remained constant at higher current levels), non-monotonic (spike rate increased with increasing current levels and then dropped below 50% of the maximum spike rate at higher current levels) and complex (both monotonic and non-monotonic rate-level characteristics) (Aitkin, 1991; Shivdasani et al., 2008). The distribution of all response types observed with single and dual-site VCN stimulation is shown in Figure 6. Regardless of single- or dual-site stimulation, and for all VCN pair types, the majority of CIC rate-level functions (> 60%) were found to be of the plateau type (Fig. 6) at both CF-aligned and CF-unaligned CIC sites. Aligned

sites exhibited higher percentages of plateau type responses than unaligned sites (Fig. 6A, 6B). Complex response types were observed less frequently at CF-aligned CIC sites than at unaligned sites for both single- and dual-site stimulation (Fig. 6A and B). Non-monotonic and monotonic response types showed only small differences when single- and dual-site stimulation were compared, and these function types represented only a small percentage of both CF-aligned and unaligned CIC sites.

Extent of activation in the CIC

For each VCN site/pair stimulated, the extent of activation in the CIC at each of six current levels was calculated: this was achieved by dividing the number of CIC sites that showed a response to VCN stimulation by the total number of CIC sites with acoustic RAs on the CIC electrode (expressed as a percentage). This was then averaged across all CIC sites and VCN pairs (Fig. 7A, E, I, and M). A 2 (stimulation type) x 6 (current level) x 3 (VCN pair type) repeated measures AVOVA was applied. For both single- and dual-site stimulation, the average extent of activation in the CIC increased with increasing current level and then saturated at higher current levels (Fig. 7A, E, I, and M). A significant difference in the total extent of CIC activation was found between single- and dual-site stimulation (Fig. 7A, E, I, and M) ($F(1,36) = 18.763$, $p < 0.0001$, ($\eta_p^2 = 0.343$)). There was a significant interaction between stimulation type and current level ($F(5,180) = 15.729$, $p < 0.0001$, ($\eta_p^2 = 0.304$)). A post-hoc simple effects analysis showed that dual-site stimulation resulted in a significantly greater extent of CIC activation than single-site stimulation at all current levels below 30 μA ($p < 0.001$). The interaction between stimulation type and VCN pair type, and the three-way interaction,

were not significant, indicating that the increase in the extent of CIC activation from dual-site stimulation was not influenced by VCN pair type.

When the extent of CIC activation was analyzed using only data from the CF-aligned CIC sites (Fig. 7B, F, J, and N), a significant main effect of stimulation type was found ($F(1,36) = 5.449$, $p < 0.03$, ($\eta_p^2 = 0.131$)). The interaction between stimulation type and current level was also significant ($F(5,180) = 12.169$, $p < 0.0001$, ($\eta_p^2 = 253$)). A post-hoc analysis showed that at current levels of 10 and 15 μA, dual-site stimulation resulted in a greater extent of activation than single-site stimulation ($p < 0.05$). No significant interaction between stimulation type and VCN pair type was observed and the three-way interaction was also non-significant.

When the extent of activation in the CIC was analyzed using only data from the CF-unaligned CIC sites (Fig. 7C, G, K, and O), a significant main effect of stimulation type was observed ($F(1,36) = 26.426$, $p < 0.0001$, ($\eta_p^2 = 0.423$)). The interaction between stimulation type and current level was also significant ($F(5,180) = 2.741$, $p < 0.03$, ($\eta_p^2 = 0.071$)). A post-hoc analysis showed that at all current levels below 30 μA, dual-site stimulation resulted in a greater extent of activation than single-site stimulation ($p < 0.001$). The interaction between stimulation type and VCN pair type, and the three-way interaction, was not significant. Overall, these results indicate that CIC sites were activated at lower thresholds by dual-site VCN stimulation, and that more CIC sites, in both CF-aligned and -unaligned frequency regions, were activated by dual-site stimulation compared to single site stimulation.

To determine whether the CF-aligned sites were preferentially activated over the CF-unaligned sites, the activation levels for the CF-unaligned sites were subtracted from those of the CF-aligned sites (Fig. 7D, H, L, and P) and a three-factor repeated measures

ANOVA was applied on the difference measures. The ANOVA revealed no significant main effect of stimulation type. However, the interaction between stimulation type and current level was found to be significant ($F(5,180) = 5.808$, $p < 0.0001$, ($\eta_p^2 = 0.139$)). A post-hoc analysis showed that dual-site stimulation resulted in a greater difference between CF-aligned and –unaligned activation compared to single-site stimulation at 10 μA ($p < 0.005$). The three-way interaction was not significant.

Further analysis was performed on CIC activation to highlight the differences between single-and dual-site stimulation, and to determine the variability across different VCN pair types. The difference in CIC activation evoked by single- and dual-site VCN stimulation was compared on a pair-by-pair basis. Figure 8 shows an example of the percentage activation of CF-unaligned sites in the CIC resulting from stimulation of two FS VCN sites, dual-site stimulation of the FS-FS pair, and the percentage change in activation obtained from dual-site stimulation (calculated as the difference in activation between the dual-site curve and the single-site curve that showed the overall greater extent of activation). In this example, the difference measure (Fig. 8; % change in extent of CIC activation resulting from dual-site stimulation) indicates that at low current levels there was an increase in activation due to dual-site stimulation (positive values), while at successively higher current levels this change in activation decreased and was zero at the highest current level presented. A summary of these dual-single difference measures resulting from stimulation of each of the VCN pairs is shown in Figure 9. Three patterns of differences in CIC activation due to dual-versus single-site VCN stimulation were observed. In most cases, dual-single activation differences were positive at low current levels and the difference was either maintained or approached zero at higher current levels (Fig. 9A and B, FS-FS pairs, n = 15, 47% of cases; Fig. 9C

and D, FS-NFS pairs, n = 21, 70%; Fig. 9E and F, NFS-NFS pairs, n = 12, 75%). In fewer cases, dual-single activation differences were around zero at low current levels and then became positive at higher current levels (Fig. 9A and B, FS-FS pairs, n = 11, 34%; Fig. 9C and D, FS-NFS pairs, n = 6, 20%; Fig. 9E and F, NFS-NFS pairs, n = 2, 12.5%). In some cases, dual-single activation differences remained around zero at most current levels (Fig. 9A and B, FS-FS pairs, n = 6, 19%; Fig. 9C and D, FS-NFS pairs, n = 3, 10%; Fig. 9E and F, NFS-NFS pairs, n = 2, 12.5%).

Frequency Specificity

With single-site stimulation, 63.8% (37/58 sites) of VCN sites were classified as frequency-specific (Figure 10). With dual-site stimulation, frequency specificity increased to 74.4% (29/39 pairs). Further analysis (Fig. 10) showed that for FS-FS VCN pairs, frequency specificity was 100% with single-site stimulation and decreased to 75% with dual-site stimulation. For FS-NFS pairs, frequency specificity with single-site stimulation was 50% and increased to 80% with dual-site stimulation. For NFS-NFS pairs, frequency specificity with single-site stimulation was zero and increased to 62.5% with dual-site stimulation.

Discussion

Using multichannel electrophysiological techniques and penetrating electrode arrays, this study showed that dual-site stimulation in similar-CF regions of the VCN was superior to single-site stimulation in terms of a number of CIC neural response measures. Dual-site stimulation resulted in decreased CIC thresholds, wider dynamic ranges, and greater extents of activation and frequency specificity. Overall, these changes indicated benefits with dual-site simulation compared to single-site stimulation; however in some cases, the effects were reversed indicating variability in outcomes. Our results showed that the changes observed with dual-site stimulation were largely dependent on the pair type (i.e., FS-FS, FS-NFS or NFS-NFS) chosen for stimulation in the VCN.

Functional Effects of Dual-site Stimulation and Organization of VCN-CIC Projections

On average, CIC sites responded to dual-site VCN stimulation with lower thresholds, wider dynamic ranges and a higher degree of frequency specificity compared to single site stimulation. The changes in thresholds and dynamic ranges were obtained with dual-site stimulation regardless of the physical separation between the stimulated VCN sites. A decrease in thresholds in the auditory cortex has been previously reported with dual-site stimulation using a CI (Bierer and Middlebrooks, 2004); this effect was attributed primarily to channel interaction owing to current summation within the cochlea. In our study, the threshold reductions, as well as wider dynamic ranges and higher extent of frequency specificity, observed with dual-site VCN stimulation may be due to integration of convergent information in the CIC from neuron populations

located within similar VCN isofrequency laminae. With the exception of NFS-NFS pairs, these effects were observed for closely- and widely-spaced VCN sites, suggesting that current summation effects in the VCN were minimal and neural convergence in the CIC is the more likely explanation for the changes observed with dual-site stimulation. For NFS-NFS pairs, there was a clear trend for the changes in thresholds and dynamic ranges from dual-site stimulation to depend on the separation between sites in the VCN, further suggesting that convergence in the CIC from multiple locations within VCN isofrequency laminae could be greater for VCN locations that are closely spaced compared to those that are spaced further apart.

A larger extent of CIC activation was observed with dual-site VCN stimulation than with single-site stimulation, particularly at lower current levels. This effect was observed in regions of the CIC that were both CF-aligned and CF-unaligned to the VCN, and was consistent with the overall lower thresholds seen with dual-site stimulation. The greater extent of CIC activation observed with dual-site VCN stimulation in our study could be important for the perception of loudness with an ABI or PABI (Moore, 2003; Zwislocki, 1995) (see later section on implications for PABI strategies). When data were analyzed on a pair-by-pair basis, the opposite effect was observed in some cases. In these instances, dual-site stimulation caused a decrease in the extent of CIC activation compared to single site stimulation, indicating that bipolar VCN stimulation is more complex than a simple one-to-one activation.

A possible explanation for the reversed effects observed with dual-site stimulation could be related to indiscriminant stimulation of auditory nerve (AN) fibers. All the animals used in this study had an intact AN, therefore it is possible that both single-and dual-site stimulation caused activation of AN fibers of passage. An intact AN allowed us to

record VCN and CIC responses to acoustic stimulation prior to electrical stimulation, and enabled neuronal CFs to be used as a basis to classify VCN pairs and to determine the frequency specificity of dual and single site VCN stimulation.

Although we only analyzed data in which CIC responses were obtained to both single- and dual-site VCN stimulation (Table 1: Group 1 response sets), it was possible, on some occasions, to deactivate sites within the CIC with dual-site VCN stimulation (Groups 4 and 5). These results suggested interactions between excitatory and inhibitory pathways within the auditory system. Evidence for such interactions has been observed in the CIC (Nayagam et al, 2005), and probably results from monosynaptic convergent input from the VCN and ogliosynaptic interactions via the ventral nucleus of the lateral lemniscus (VNLL) which provides strong inhibitory input to the CIC. In some cases, dual-site stimulation may have evoked sufficient activation of VNLL neurons which, in turn, resulted in substantial inhibition of CIC neurons. This effect may be compounded by the VNLL's lack of tonotopicity and its various cells types that integrate information across and within multiple frequency regions (Nayagam et al., 2006). Further research is necessary to investigate the existence, distribution, and functional implications of these excitatory and inhibitory pathways for prosthetic stimulation with an ABI.

Lastly, our previous study (Shivdasani et al., 2008) indicated that the location of the stimulating array in the VCN can influence CIC thresholds and frequency specificity. Although outside the scope of this study, it will be important to assess the impact of the location of VCN stimulation on CIC responses using both single-and multi-site stimulation.

Implications for Penetrating Auditory Brainstem Implant Strategies

The main implication of our results for the design of the PABI pertains to the current levels used in present stimulation strategies. In present ABIs and PABIs, each VCN electrode is stimulated with a current level based on the amplitude of the frequency components coded by the speech processor. The current level used for stimulation is normally chosen between pre-determined levels required for perception threshold and for producing a comfortable sensation, commonly referred to as the T and C levels, respectively (Lesinski-Schiedat et al., 2000). Although likely, it is unclear whether the perception of loudness is directly correlated with the extent of neural activation in the CIC (Moore, 2003; Zwislocki, 1995). If the T and C current levels used for perception are higher than those required for threshold and saturation of neural activation in the CIC, then frequency specificity might be compromised at these high current levels. This could, in turn, result in an alteration of the perceived frequency and therefore decrease the effectiveness of encoding frequency information at the expense of coding for loudness. One would presume, based on our results, that stimulating more sites within VCN isofrequency laminae, using relatively lower currents on individual-sites, might allow both adequate neural activation in the CIC for perception of loudness, as well as maintaining frequency specificity. Consequently, the technique of multi-site VCN stimulation within isofrequency laminae should be taken into account when developing any new stimulation strategies for the PABI.

A second implication of dual-site stimulation is the impact of VCN pair type on the various parameters analyzed. Our data show that with a total of 58 usable VCN sites, we were more likely to find an FS site (n = 37) rather than a NFS site (n = 21). Therefore, if

a clinical electrode design incorporated multiple sites in each VCN isofrequency lamina, then there would be a higher probability of choosing FS-NFS pairs (P = 0.47; calculated using probability of dependent events) compared to FS-FS (P = 0.4) and NFS-NFS (P = 0.13) pairs for dual-site stimulation. While stimulating FS-FS pairs provides benefits in terms of lower thresholds and wider dynamic ranges, there is a significant trade-off in the decreased extent of activation in the CIC and frequency specificity. FS-NFS and NFS-NFS pairs are more likely to result in higher frequency specificity, as well as having the added benefit of decreased thresholds and increased dynamic ranges with minimal trade-offs. We propose that further research is necessary to devise a clinical method of identifying FS and NFS sites in the VCN so that appropriate pairs of electrode sites can be chosen for dual-site stimulation and unwanted effects are avoided.

Lastly, it will be important to perform a similar study to assess the level of VCN-CIC convergence and the effects of multi-site VCN stimulation in animals without the presence of the AN. The main goal of this study was to assess if localized, frequency-specific CIC activation with low thresholds and wide dynamic ranges was achievable and was a first step towards implementing multi-site VCN stimulation. Many ABI candidates may have had normal hearing up until tumor removal and some residual hearing after tumor removal (Briggs et al., 2000; Vincenti et al., 2008). In addition, patient groups with an intact AN, such as those with cochlear ossification and possibly those with bacterial meningitis, can benefit from an ABI (Colletti et al., 2009; Grayeli et al., 2007). If we cannot achieve favorable properties in a normal hearing system using multi-site VCN stimulation, then it will be more difficult to achieve them in a deafened system.

In conclusion, while our results have provided insights into the complexity of multi-site VCN stimulation, they suggest that stimulation of only two sites within similar isofrequency laminae may not be sufficient to evoke appropriate patterns of neural activity within the CIC. Simultaneous or sequential stimulation of several sites within each frequency lamina might be required. Incorporating multi-site VCN stimulation techniques should enable higher-order auditory structures to encode frequency and loudness information more effectively, and therefore result in improved speech perception.

Acknowledgements

We thank Prof. Dexter Irvine and Dr. Janine Clarey who provided valuable edits on previous versions of this manuscript. We thank Dr. Conor Hogan from the Chemistry department at La Trobe University for assistance in electrochemical activation of the electrodes. We also thank Ayla Barutchu for assistance with the statistical analyses and Courtney Suhr for technical assistance. This research was conducted at the School of Psychological Science at La Trobe University and at the Auditory Clinical Neuroscience Unit, The Bionic Ear Institute, Melbourne, Australia. Funding was provided by the Garnett Passe & Rodney Williams Memorial Foundation and La Trobe University. The Bionic Ear Institute acknowledges the support it receives from the Victorian Government through its Operational Infrastructure Support Program.

References

Aitkin L. 1991. Rate-level functions of neurons in the inferior colliculus of cats measured with the use of free-field sound stimuli. J Neurophysiol 65(2):383-392.

Anderson DJ, Najafi K, Tanghe SJ, Evans DA, Levy KL, Hetke JF, Xue XL, Zappia JJ, Wise KD. 1989. Batch-fabricated thin-film electrodes for stimulation of the central auditory system. IEEE Trans Biomed Eng 36(7):693-704.

Beebe X, Rose TL. 1988. Charge injection limits of activated iridium oxide electrodes with 0.2 ms pulses in bicarbonate buffered saline. IEEE Trans Biomed Eng 35(6):494-495.

Bierer JA, Middlebrooks JC. 2004. Cortical responses to cochlear implant stimulation: channel interactions. J Assoc Res Otolaryngol 5(1):32-48.

Briggs RJ, Fabinyi G, Kaye AH. 2000. Current management of acoustic neuromas: review of surgical approaches and outcomes. J Clin Neurosci 7(6):521-526.

Colletti V, Carner M, Miorelli V, Colletti L, Guida M, Fiorino F. 2004a. Auditory brainstem implant in posttraumatic cochlear nerve avulsion. Audiol Neurootol 9(4):247-255.

Colletti V, Carner M, Miorelli V, Guida M, Colletti L, Fiorino F. 2004b. Cochlear implant failure: is an auditory brainstem implant the answer? Acta Otolaryngol 124(4):353-357.

Colletti V, Carner M, Miorelli V, Guida M, Colletti L, Fiorino F. 2005. Auditory brainstem implant (ABI): new frontiers in adults and children. Otolaryngol Head Neck Surg 133(1):126-138.

Colletti V, Fiorino FG, Carner M, Miorelli V, Guida M, Colletti L. 2004c. Auditory brainstem implant as a salvage treatment after unsuccessful cochlear implantation. Otol Neurotol 25(4):485-496; discussion 496.

Colletti V, Shannon R, Carner M, Veronese S, Colletti L. 2009. Outcomes in Nontumor Adults Fitted With the Auditory Brainstem Implant: 10 Years' Experience. Otol Neurotol.

Colletti V, Shannon RV. 2005. Open set speech perception with auditory brainstem implant? Laryngoscope 115(11):1974-1978.

DiCarlo JJ, Lane JW, Hsiao SS, Johnson KO. 1996. Marking microelectrode penetrations with fluorescent dyes. J Neurosci Methods 64(1):75-81.

El-Kashlan HK. 1999. Multichannel cochlear nucleus stimulation. Otolaryngol Head Neck Surg 121(3):169-175.

El-Kashlan HK, Niparko JK, Altschuler RA, Miller JM. 1991. Direct electrical stimulation of the cochlear nucleus: surface vs. penetrating stimulation. Otolaryngol Head Neck Surg 105(4):533-543.

Friesen LM, Shannon RV, Baskent D, Wang X. 2001. Speech recognition in noise as a function of the number of spectral channels: comparison of acoustic hearing and cochlear implants. J Acoust Soc Am 110(2):1150-1163.

Grayeli AB, Kalamarides M, Bouccara D, Ben Gamra L, Ambert-Dahan E, Sterkers O. 2007. Auditory brainstem implantation to rehabilitate profound hearing loss with totally ossified cochleae induced by pneumococcal meningitis. Audiol Neurootol 12(1):27-30.

Hernandez O, Espinosa N, Perez-Gonzalez D, Malmierca MS. 2005. The inferior colliculus of the rat: a quantitative analysis of monaural frequency response areas. Neuroscience 132(1):203-217.

Hinkle DE, Wiersma W, Jurs SG. 1998. Analysis of Variance, Two-Way Classification. Applied Statistics for the Behavioral Sciences. 4 ed: Houghton Mifflin Company. p 417-460.

Jackson KB, Mark G, Helms J, Mueller J, Behr R. 2002. An auditory brainstem implant system. Am J Audiol 11(2):128-133.

Koppl C, Yates G. 1999. Coding of sound pressure level in the barn owl's auditory nerve. J Neurosci 19(21):9674-9686.

Kuchta J. 2007. Twenty-five years of auditory brainstem implants: perspectives. Acta Neurochir Suppl 97(Pt 2):443-449.

Kuchta J, Otto SR, Shannon RV, Hitselberger WE, Brackmann DE. 2004. The multichannel auditory brainstem implant: how many electrodes make sense? J Neurosurg 100(1):16-23.

Lesinski-Schiedat A, Frohne C, Illg A, Rost U, Matthies C, Battmer RD, Samii M, Lenarz T. 2000. Auditory brainstem implant in auditory rehabilitation of patients with neurofibromatosis type 2: Hannover programme. J Laryngol Otol Suppl(27):15-17.

Lim HH, Anderson DJ. 2007. Antidromic activation reveals tonotopically organized projections from primary auditory cortex to the central nucleus of the inferior colliculus in guinea pig. J Neurophysiol 97(2):1413-1427.

Liu X, McPhee G, Seldon HL, Clark GM. 1997. Acute study on the neuronal excitability of the cochlear nuclei of the guinea pig following electrical stimulation. Acta Otolaryngol 117(3):363-375.

Liu X, Seldon HL, Clark GM. 1998. Chronic study on the neuronal excitability of the cochlear nuclei of the cat following electrical stimulation. Acta Otolaryngol 118(4):524-529.

Loizou PC, Dorman M, Fitzke J. 2000. The effect of reduced dynamic range on speech understanding: implications for patients with cochlear implants. Ear Hear 21(1):25-31.

Loizuo PC. 1998 Mimicking the human ear. IEEE Signal Processing Magazine:101-130.

Mauger SJ, Shivdasani MN, Rathbone GD, Argent RE, Paolini AG. 2010. An *in vivo* investigation of first spike latencies in the inferior colliculus in response to multichannel penetrating auditory brainstem implant stimulation. J Neural Eng (In Press).

McCreery D, Lossinsky A, Pikov V. 2007. Performance of multisite silicon microprobes implanted chronically in the ventral cochlear nucleus of the cat. IEEE Trans Biomed Eng 54(6 Pt 1):1042-1052.

McCreery DB. 2008. Cochlear nucleus auditory prostheses. Hear Res 242(1-2):64-73.

McCreery DB, Agnew WF, Yuen TG, Bullara L. 1990. Charge density and charge per phase as cofactors in neural injury induced by electrical stimulation. IEEE Trans Biomed Eng 37(10):996-1001.

McCreery DB, Shannon RV, Moore JK, Chatterjee M. 1998. Accessing the tonotopic organization of the ventral cochlear nucleus by intranuclear microstimulation. IEEE Trans Rehabil Eng 6(4):391-399.

Moore BC. 2003. Coding of sounds in the auditory system and its relevance to signal processing and coding in cochlear implants. Otol Neurotol 24(2):243-254.

Nayagam DA, Clarey JC, Paolini AG. 2005. Powerful, onset inhibition in the ventral nucleus of the lateral lemniscus. J Neurophysiol 94(2):1651-1654.

Nayagam DA, Clarey JC, Paolini AG. 2006. Intracellular responses and morphology of rat ventral complex of the lateral lemniscus neurons in vivo. J Comp Neurol 498(2):295-315.

Niparko JK, Altschuler RA, Evans DA, Xue XL, Farraye J, Anderson DJ. 1989a. Auditory brainstem prosthesis: biocompatibility of stimulation. Otolaryngol Head Neck Surg 101(3):344-352.

Niparko JK, Altschuler RA, Xue XL, Wiler JA, Anderson DJ. 1989b. Surgical implantation and biocompatibility of central nervous system auditory prostheses. Ann Otol Rhinol Laryngol 98(12 Pt 1):965-970.

Nizami L. 2002. Estimating auditory neuronal dynamic range using a fitted function. Hear Res 167(1-2):13-27.

Nobbe A, Schleich P, Zierhofer C, Nopp P. 2007. Frequency discrimination with sequential or simultaneous stimulation in MED-EL cochlear implants. Acta Otolaryngol:1-7.

Otto SR, Brackmann DE, Hitselberger WE, Shannon RV, Kuchta J. 2002. Multichannel auditory brainstem implant: update on performance in 61 patients. J Neurosurg 96(6):1063-1071.

Otto SR, Shannon RV, Brackmann DE, Hitselberger WE, Staller S, Menapace C. 1998. The multichannel auditory brain stem implant: performance in twenty patients. Otolaryngol Head Neck Surg 118(3 Pt 1):291-303.

Otto SR, Shannon RV, Wilkinson EP, Hitselberger WE, McCreery DB, Moore JK, Brackmann DE. 2008. Audiologic Outcomes With the Penetrating Electrode Auditory Brainstem Implant. Otol Neurotol 29(8):1147-1154.

Paxinos G, Watson C. 2007. The Rat Brain in Stereotaxic Coordinates. 6th Edition, San Diego: Academic Press.

Portfors CV, Felix RA, 2nd. 2005. Spectral integration in the inferior colliculus of the CBA/CaJ mouse. Neuroscience 136(4):1159-1170.

Sachs MB, Abbas PJ. 1974. Rate versus level functions for auditory-nerve fibers in cats: tone-burst stimuli. J Acoust Soc Am 56(6):1835-1847.

Sachs MB, Winslow RL, Sokolowski BH. 1989. A computational model for rate-level functions from cat auditory-nerve fibers. Hear Res 41(1):61-69.

Schwartz MS, Otto SR, Shannon RV, Hitselberger WE, Brackmann DE. 2008. Auditory brainstem implants. Neurotherapeutics 5(1):128-136.

Shannon RV, Fu QJ, Galvin J, 3rd. 2004. The number of spectral channels required for speech recognition depends on the difficulty of the listening situation. Acta Otolaryngol Suppl(552):50-54.

Shivdasani MN, Mauger SJ, Rathbone GD, Paolini AG. 2008. Inferior colliculus responses to multichannel microstimulation of the ventral cochlear nucleus: implications for auditory brainstem implants. J Neurophysiol 99(1):1-13.

Shivdasani MN, Mauger SJ, Rathbone GD, Paolini AG. 2009. Neural synchrony in ventral cochlear nucleus neuron populations is not mediated by intrinsic processes but is stimulus induced: implications for auditory brainstem implants. J Neural Eng 6(6):65003.

Stickney GS, Loizou PC, Mishra LN, Assmann PF, Shannon RV, Opie JM. 2006. Effects of electrode design and configuration on channel interactions. Hear Res 211(1-2):33-45.

Sutter ML, Schreiner CE. 1991. Physiology and topography of neurons with multipeaked tuning curves in cat primary auditory cortex. J Neurophysiol 65(5):1207-1226.

Takahashi H, Nakao M, Kaga K. 2005. Accessing ampli-tonotopic organization of rat auditory cortex by microstimulation of cochlear nucleus. IEEE Trans Biomed Eng 52(7):1333-1344.

Vincenti V, Pasanisi E, Guida M, Di Trapani G, Sanna M. 2008. Hearing rehabilitation in neurofibromatosis type 2 patients: cochlear versus auditory brainstem implantation. Audiol Neurootol 13(4):273-280.

Yates GK, Manley GA, Koppl C. 2000. Rate-intensity functions in the emu auditory nerve. J Acoust Soc Am 107(4):2143-2154.

Yates GK, Winter IM, Robertson D. 1990. Basilar membrane nonlinearity determines auditory nerve rate-intensity functions and cochlear dynamic range. Hear Res 45(3):203-219.

Zeng FG, Galvin JJ, 3rd. 1999. Amplitude mapping and phoneme recognition in cochlear implant listeners. Ear Hear 20(1):60-74.

Zwislocki JJ. 1995. Cochlear precursors of neural pitch and loudness codes. Ann Otol Rhinol Laryngol Suppl 166:12-15.

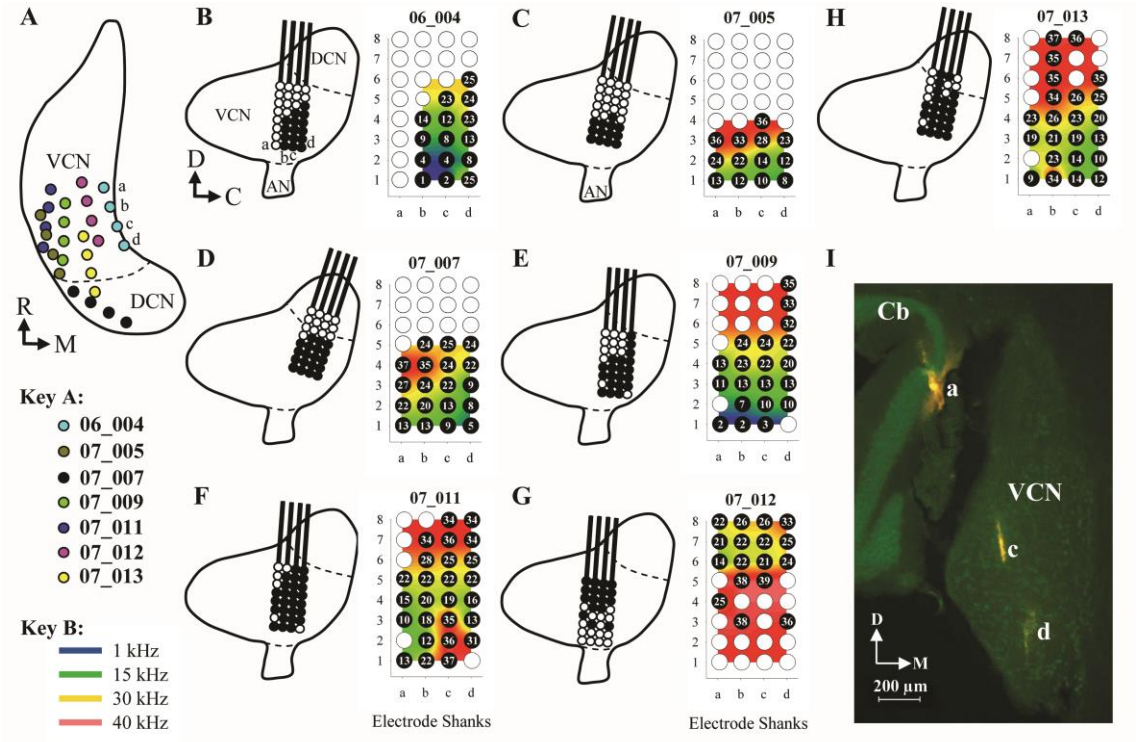

Figure 1. VCN electrode placements, tonotopic maps and an example of histological verification of electrode locations. (A) Placement of electrode shanks into the cochlear nucleus (CN) is shown in the horizontal plane and was verified by histological analysis in all seven animals (Key A). (B-H) Parasagittal representation of the same experiments in (A) showing the different regions of the CN (AN, Auditory Nerve; VCN, Ventral Cochlear Nucleus; DCN, Dorsal Cochlear Nucleus) in relation to electrode shank placements. The tonotopic map obtained in each animal is shown alongside. Each of the four shanks is represented by a letter (a-d, 'a' is most rostral, 'd' is most caudal) and the electrode sites are numbered from 1-8. The colors represent the frequency gradient, with high frequencies shown in red and low frequencies shown in blue (Key B). Each circle in the tonotopic maps and parasagittal diagrams represents a recording site on the electrode. The numbers in the circles indicate the CF of the multiunit cluster at that site. Electrode sites that were not used for stimulation are indicated by the open circles in the parasagittal diagrams. (I) Photomicrograph (x4 magnification) of a coronal brain section

from Exp 07_013 showing the VCN and part of the cerebellum (Cb). The electrode tracks for three of the four shanks (shanks a, c and d) are marked with fluorescent DiI stain (yellow) and are clearly discernable; the section was counterstained for Nissl substance (green).

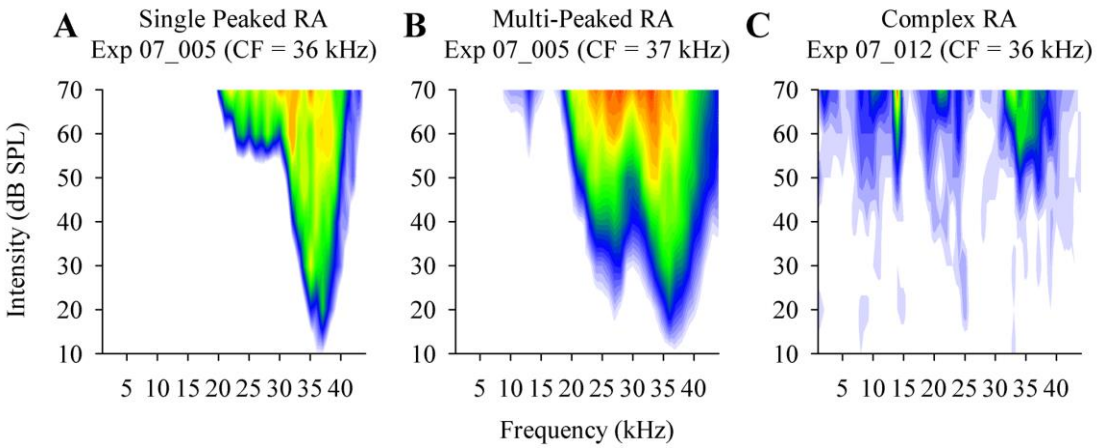

Figure 2. Examples of acoustic RAs recorded from CIC neurons. (A) A single peaked RA with a CF of 36 kHz in experiment 07_005. (B) A multi-peaked RA with a CF of 37 kHz recorded in experiment 07_005. Note there is a higher threshold peak at 27 kHz. (C) A complex RA with a CF of 36 kHz recorded in experiment 07_012. Colors indicate normalized spike rate, with maximum spike rate shown in red and minimum spike rate shown in blue.

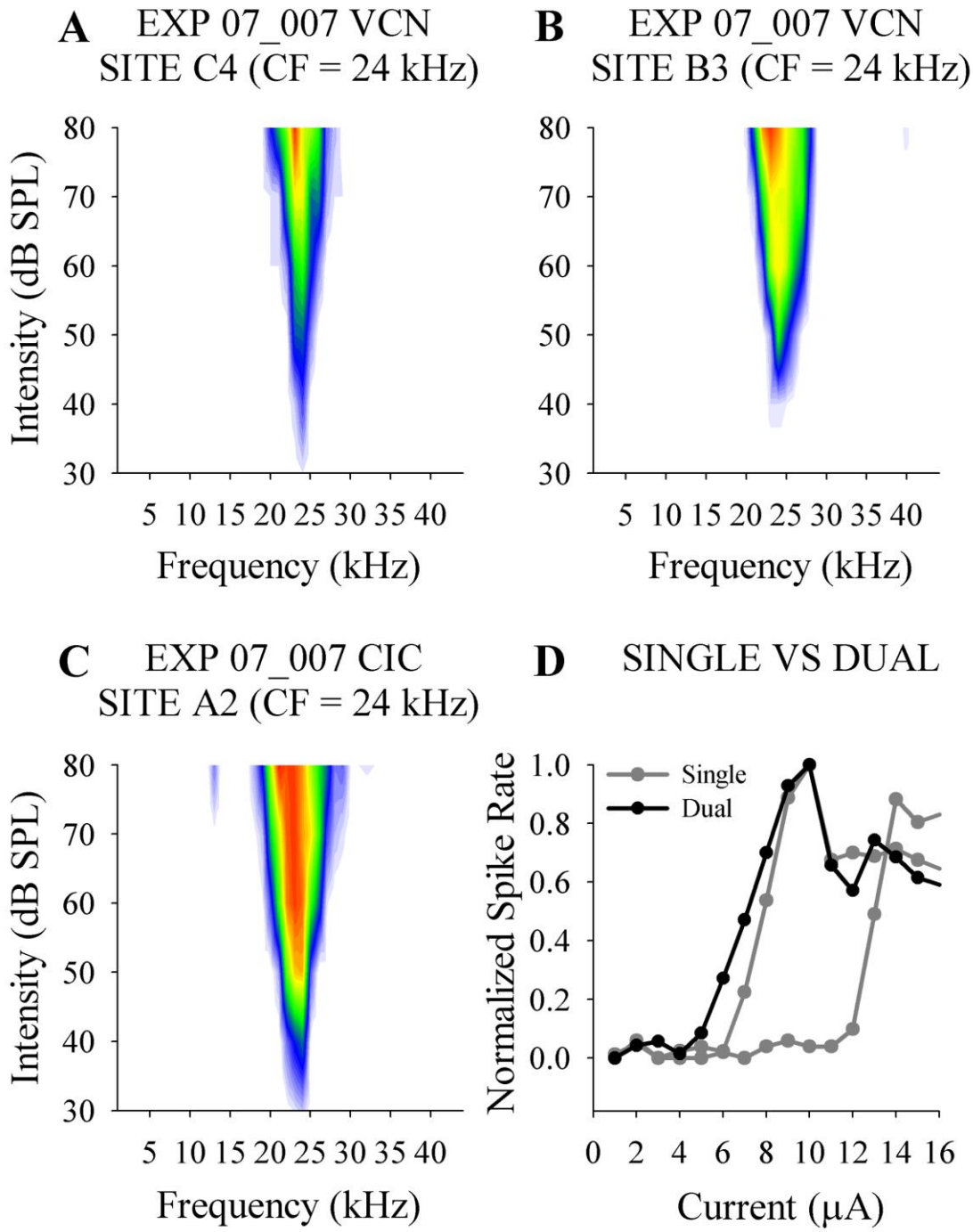

Figure 3. An example of threshold improvement with dual-site stimulation. (A and B) Acoustic RAs with similar CFs (24 kHz) at two VCN sites (c4 and b3) in experiment 07_007 (tonotopic map shown in Fig. 1D). (C) Acoustic RA of a CF-aligned CIC site (a2, CF = 24 kHz) from the same experiment. Colors indicate normalized spike rate with maximum spike rate shown in red and minimum shown in blue. (D) Normalized

rate-level functions at CIC site a2 in response to single (grey lines/circles) and dual-site (black line/circles) stimulation of VCN sites c4 and b3) dual-site. Note reduction in response threshold with dual-site stimulation.

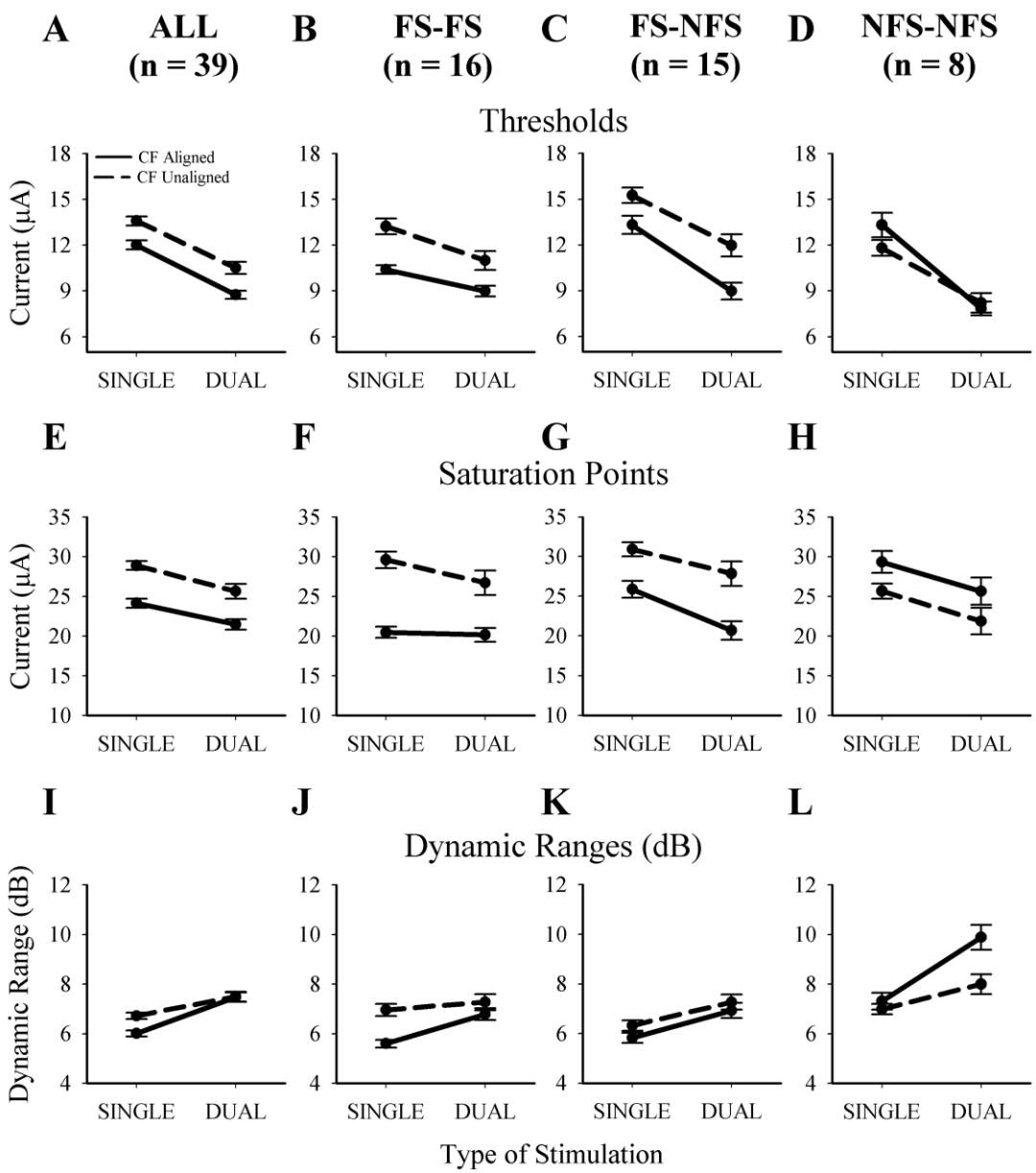

Figure 4. Effect of dual-site stimulation on average CIC thresholds, saturation points and dynamic ranges. The average (± SEM) thresholds, saturation points and dynamic ranges of CIC sites are plotted for single- versus dual-site stimulation for all VCN pairs (A, E, I; n = 39), and for each individual pair type [FS-FS (B, F, J; n= 16), FS-NFS (C, G, K; n = 15) and NFS-NFS (D, H, L; n = 8)]. Data are plotted for both CF-aligned (solid lines) and CF-unaligned (dashed lines) CIC sites.

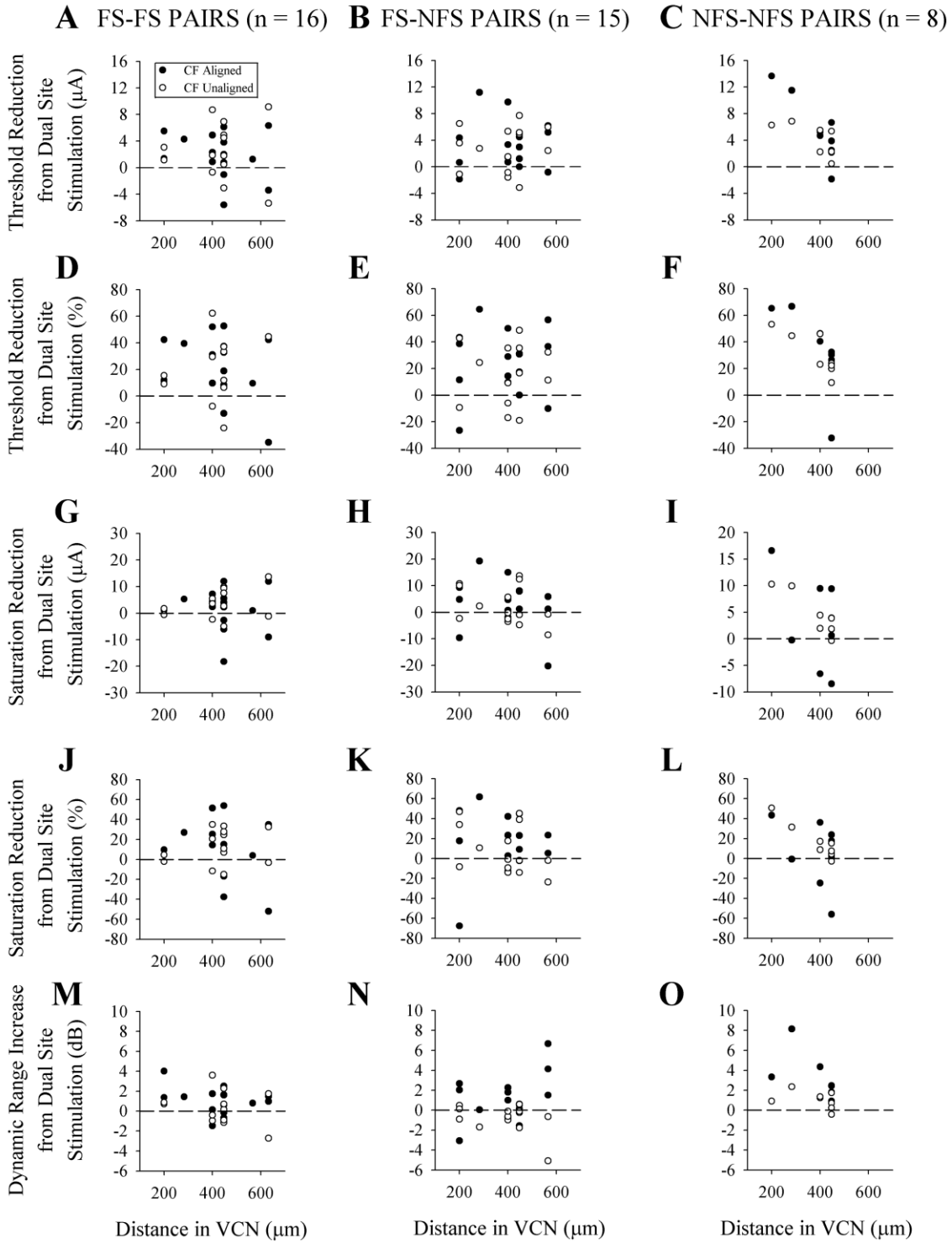

Figure 5. Effect of physical separation of individual stimulation sites in a VCN pair on CIC threshold and dynamic range improvements obtained with dual-site stimulation. Reduction in mean thresholds resulting from dual-site stimulation is measured in μA and expressed as a percentage (respectively, A-C and D-F) for CF-aligned (closed

circles) and CF-unaligned (open circles) CIC sites and is plotted against separation in the VCN (μm). Similarly, reductions in saturation points (G-I and J-L) and increases in dynamic ranges (M-O) from dual-site stimulation are plotted against separation (μm). Data are shown for all three VCN pair types (left column, FS-FS; middle column, FS-NFS; right column, NFS-NFS). Dashed lines represent no change with dual-site stimulation.

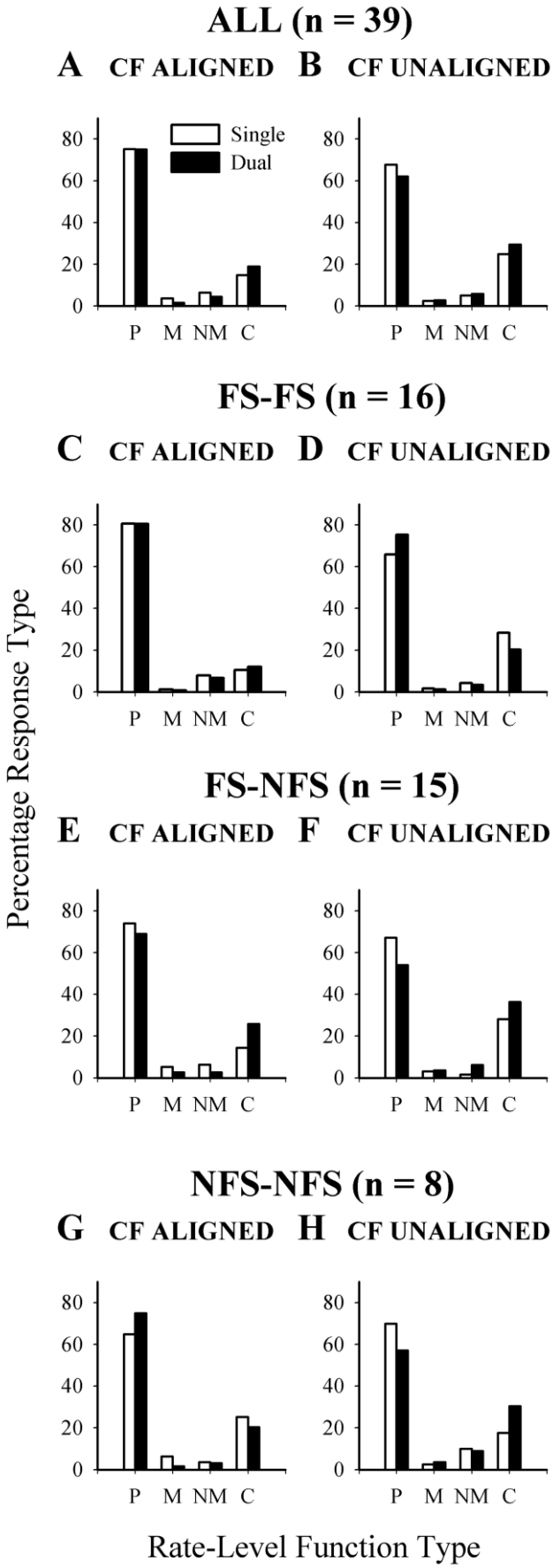
ALL (n = 39)
A CF ALIGNED
B CF UNALIGNED
Single
Dual
FS-FS (n = 16)
C CF ALIGNED
D CF UNALIGNED
FS-NFS (n = 15)
E CF ALIGNED
F CF UNALIGNED
NFS-NFS (n = 8)
G CF ALIGNED
H CF UNALIGNED
0
20
40
60
80
P M NM C
Percentage Response Type
Rate-Level Function Type

Figure 6. Effect of dual-site stimulation on CIC rate-level functions. (A and B) Percentage distribution of CIC rate-level function types for all CF-aligned and CF-unaligned sites and the effect of single versus dual-site stimulation. Data are shown for each VCN pair type (C and D, FS-FS; E and F, FS-NFS; G and H, NFS-NFS). Abbreviations: C, complex; M, monotonic; NM, nonmonotonic; P, plateau.

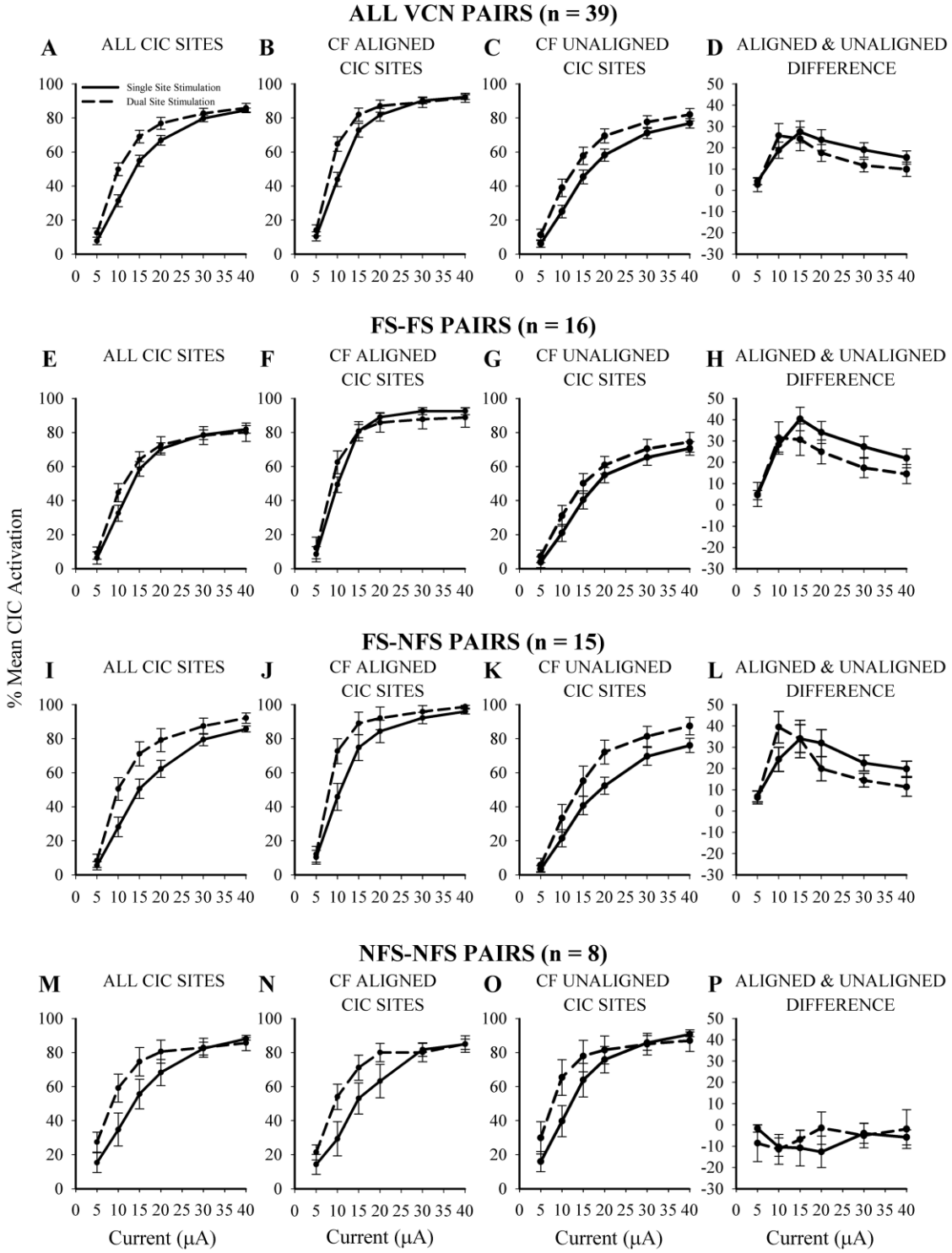

Figure 7. Effect of dual-site stimulation on the extent of CIC activation. Mean (± SEM) extent of CIC activation was calculated at various current levels for all VCN pairs stimulated. (A) CIC sites that responded to electrical stimulation expressed as a percentage of the total number of possible CIC sites. (B) CF-aligned sites that

responded expressed as a percentage of the total number of CF-aligned sites. (C) CF-unaligned sites that responded expressed as a percentage of the total number of CF-unaligned sites. (D) Difference between CF-aligned and CF-unaligned CIC activation. Solid lines show data from single-site stimulation; dashed lines indicate dual-site stimulation. The same analysis is shown for each VCN pair type: FS-FS (panels E-H), FS-NFS (panels I-L) and NFS-NFS (panels M-P).

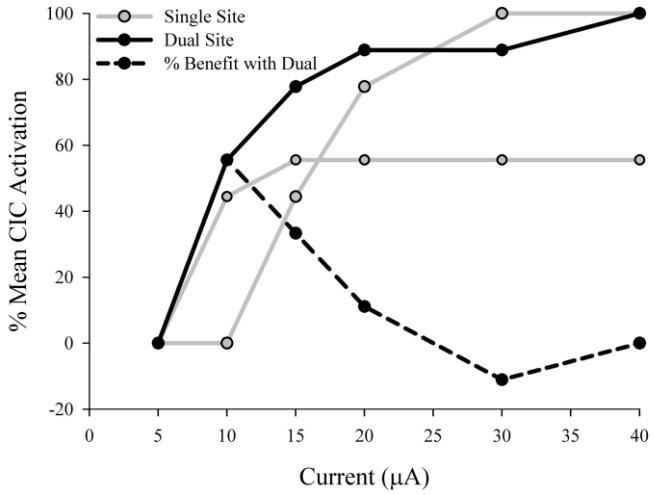

Figure 8. Example of the difference in CIC activation between single-and dual- site VCN stimulation. Graph shows CIC activation at each current level resulting from stimulation of two single sites (solid gray lines), dual-site stimulation (solid black line), and the percentage change in activation due to dual-site stimulation (dashed black line). The change in activation was calculated by subtracting the single site stimulation curve that showed the overall greater extent of activation from the dual-site stimulation curve.

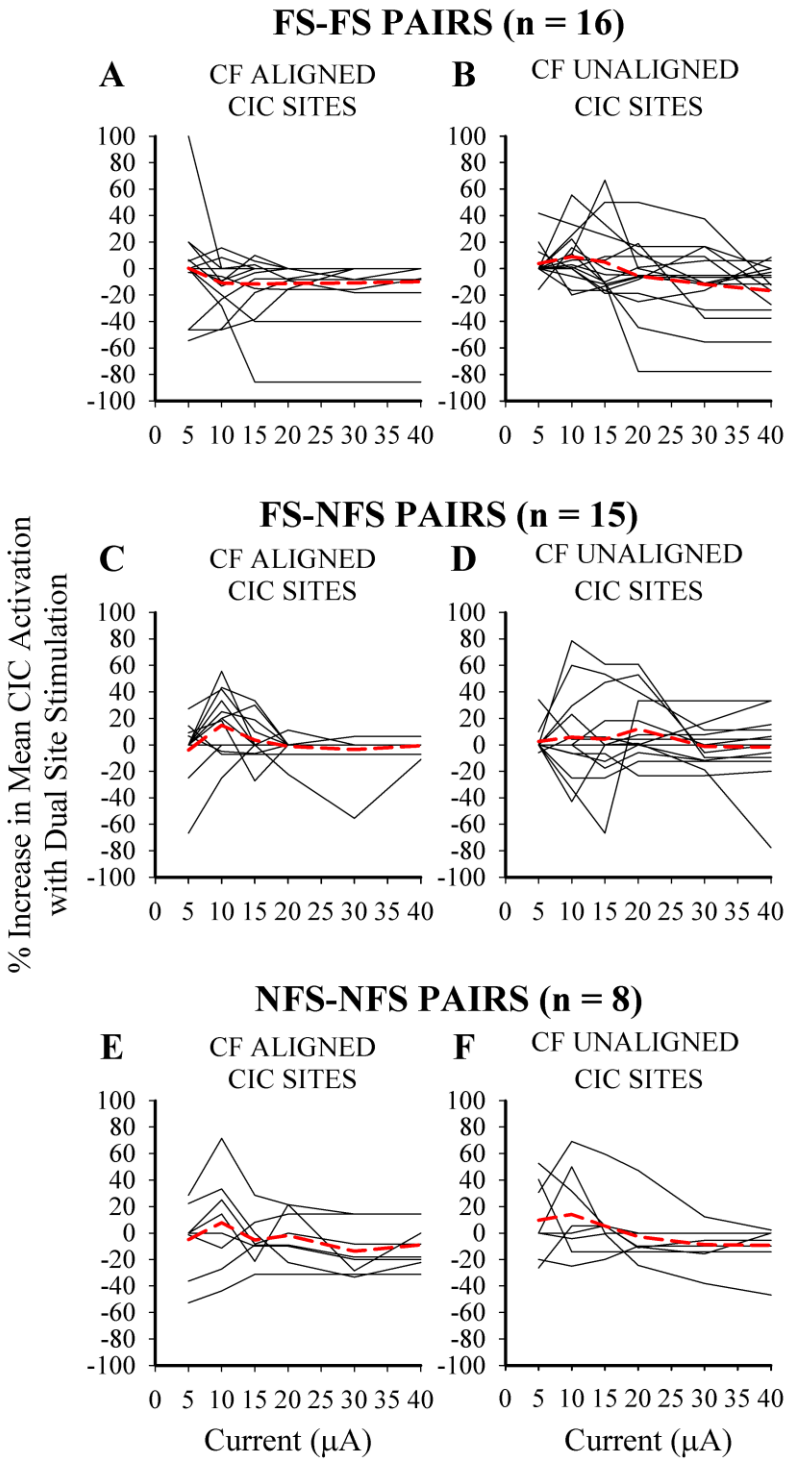

Figure 9. Dual-single activation differences in the CIC. The increase in CIC activation due to dual-site stimulation is plotted for each current level for individual FS-FS VCN pairs. Data are shown for CF-aligned (A) and CF-unaligned (B) CIC sites. Similar data are shown for stimulation of the FS-NFS (C and D) and NFS-NFS (E and F) VCN pairs.

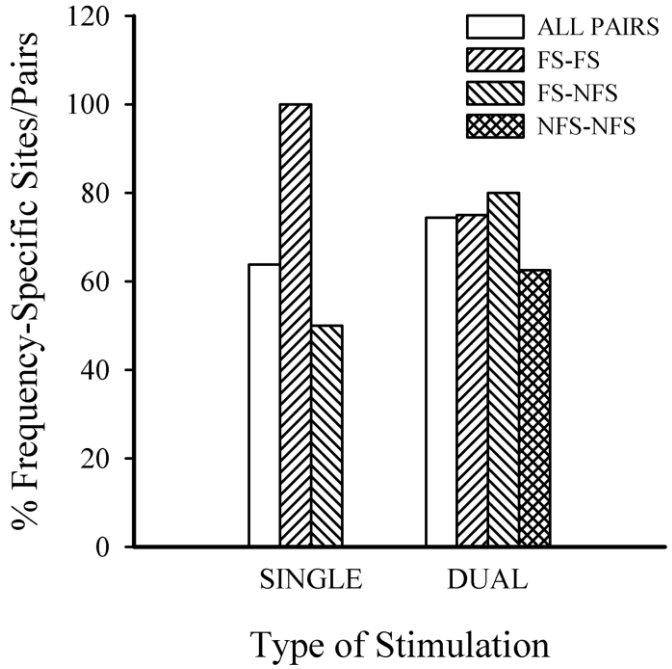

Figure 10. Effect of dual-site stimulation on VCN frequency specificity. Bar graph shows percentage VCN frequency specificity resulting from single and dual-site stimulation. Data is shown for all VCN pairs (n = 39; open bars) as well as for each VCN pair type. The FS-FS (n=16) pairs showed a decrease in specificity, while the FS-NFS (n=15) and NFS-NFS (n=8) pairs showed an increase in specificity with dual-site stimulation.

Table 1. *Classification of CIC response sets into five groups*

GROUP	STIMULATION OF VCN SITE A	STIMULATION OF VCN SITE B	DUAL-SITE STIMULATION	TOTAL RESPONSE SETS	CF ALIGNED SETS	CF UNALIGNED SETS
Group 1	R	R	R	606	312	294
Group 2	R	NR	R	142	53	89
Group 3	R	NR	NR	77	13	64
Group 4	R	R	NR	40	17	23
Group 5	NR	NR	R	20	7	13
R = Response NR = No Response				**885**	**402**	**483**

Table 1